ACS Catalysis

Article

Yin and Yang Dual Characters of CuOx Clusters for C–C Bond Oxidation Driven by Visible Light

Tingting Hou, Nengchao Luo, Hongji Li, Marc Heggen, Jianmin Lu, Yehong Wang, and Feng Wang

ACS Catal., **Just Accepted Manuscript** • Publication Date (Web): 24 Apr 2017

Yin and Yang Dual Characters of CuO_x Clusters for C–C Bond Oxidation Driven by Visible Light

Tingting Hou,[a,b] Nengchao Luo,[a,b] Hongji Li,[a,b] Marc Heggen,[c] Jianmin Lu,[a] Yehong Wang,[a] and Feng Wang*[a]

[a] State Key Laboratory of Catalysis, Dalian National Laboratory for Clean Energy, Dalian Institute of Chemical Physics, Chinese Academy of Sciences, Dalian 116023, P. R. China

[b] University of Chinese Academy of Sciences, Beijing 100049, P. R. China

[c] Ernst Ruska Centre for Microscopy and Spectroscopy with Electrons and Peter Grünberg Institute, Forschungszentrum Juelich GmbH, Juelich 52425, Germany

*Corresponding author: Feng Wang

Tel: +86-411-84379762; Fax: +86-411-84379798

E-mail: wangfeng@dicp.ac.cn

ABSTRACT

Selective cleavage of C–C bond is pursued as a useful chemical transformation method in biomass utilization. Herein, we report a hybrid CuO_x/ceria/anatase nanotubes catalyst in the selective oxidation of C–C bond under visible light irradiation. Using lignin β-1 model as substrate offers 96% yields of benzaldehydes. Characterized results by high angle annular dark field-scanning transmission electron microscopy (HAADF-STEM) and energy-dispersive X-ray spectroscopy-element (EDX) mapping reveal that CuO_x clusters are highly dispersed on the exposed anatase surface as well as on the nanosized ceria domains. In-depth investigations by Raman, and ultraviolet-visible (UV-vis) spectroscopy, together with density functional theory (DFT) calculation further verify the CuO_x clusters present on the ceria domains increase the concentration of surface defects (Ce^{3+} ions and oxygen vacancies) and accordingly improve the photocatalytic activity (Yang character); the CuO_x clusters decorating on anatase suppress the side reaction (oxy-dehydrogenation without C–C bond cleavage) because of upward shifting the valence band (VB) edge of anatase (Yin character). A hydrogen-abstraction from β-carbon by photogenerated holes is a vital step in the conversion.

KEYWORDS: heterogeneous catalysis, visible light, ceria, copper, titania, C–C bond, benzaldehyde

INTRODUCTION

Selective oxidation of C–C bond is a significant process to produce oxygenates.[1] As an alternative and sustainable feedstock, lignin accounts for around 30% weight of lignocellulosic biomass.[2] The presence of C–C bond is one of the reasons for lignin's recalcitrance to be converted into monomers. As a typical C–C bond, the β-1 linkage connects two phenyl groups by replacement of the O-bound phenoxy unit with a C-bound aryl group (Scheme 1). Baker and Hanson et al. have reported the cleavage of β-1 bond over a copper (I) trifluoromethanesulfonate catalyst assisted by 10 mol % of 2,2,6,6-tetramethyl-1-piperidinyloxy (TEMPO) and 10 equivalent of 2,6-lutidine.[3] Shi's group has developed a protocol to fragment lignin β-1 models using sodium persulfate as oxidant at 100 °C.[4] Very recently, our group has reported a $Cu(OAc)_2/BF_3{\cdot}OEt_2$ catalytic system for C–C bond cleavage in β-1 ketones.[5] However, a facile and efficient catalytic system that can achieve the lignin β-1 C–C bond cleavage is desired but far less developed.

Photocatalytic process holds great promise to reduce the energy consumption in organic reactions[6] and has attracted broad interests.[7] It will be of significance to realize the photolysis of lignin into monomers under mild conditions.[8] When C–C bond is a targeted linkage to be cleaved, the activation of the C_β–H bond is a requisite (Scheme 1).[9] But once the C–OH bond is converted to a ketone via oxy-dehydrogenation, the C_α–C_β bond dissociation energy (BDE) increases from 294.7 to 354.2 kJ/mol, and consequently the formed ketone is more difficult to be converted. This is different with the cleavage of β-O-4 bond that is easier to be

cleaved once the C–OH bond is pre-oxidized to ketone.[8a, 10] Thus, a highly selective catalyst to oxidize β-1 C–C bond should selectively activate C_{β}–H bond but suppress the formation of ketone. This has been rarely achieved in heterogeneous photocatalysis.[11]

Scheme 1. Oxy-dehydrogenation reaction competes with C–C cleavage reaction in the oxidation of β-1 model.

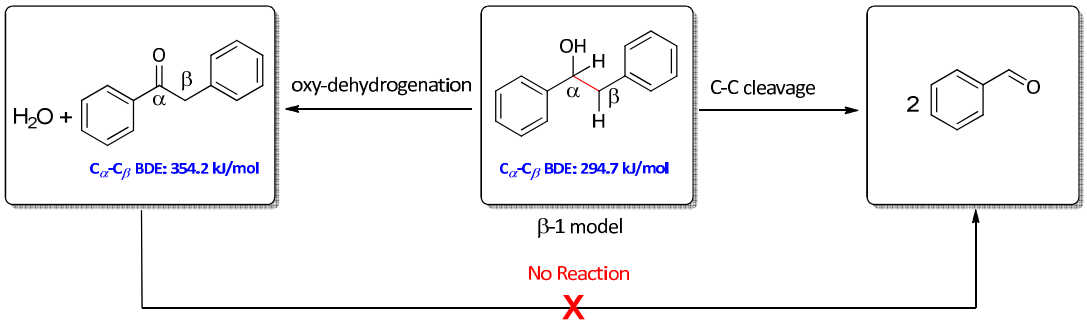

We herein report the bifunctionality of CuO_x clusters in the photolysis of C–C bond, especially in lignin β-1 model. Catalytic results show that decoration of CuO_x clusters on ceria/anatase significantly promotes the C–C bond cleavage with 98% selectivity of benzaldehyde under visible light. The reaction mechanism involves a hydrogen abstraction from a benzylic carbon (β-C) process by the photogenerated holes, which is supported by control experiments and kinetic isotope effects (KIE) investigations. Detailed studies, including X-ray diffraction (XRD), HAADF-STEM, EDX-mapping, physical absorption, Raman, and UV-vis spectroscopy as well as DFT calculation reveal that the highly dispersed CuO_x clusters have dual characters on both

ceria domains and exposed anatase nanotubes, i.e. promoting the C–C bond cleavage (Yang character), and inhibiting unwanted oxy-dehydrogenation reaction (Yin character).[12] This study attains selective C–C bond oxidation to benzaldehydes, particularly in the presence of competitive ketone formation reaction, using photoenergy by controlling the decoration location of CuO_x clusters. Although copper catalysts have been known in activating C–C bonds,[9b] such dual characters of CuO_x clusters in heterogeneous catalysis are very rare.

EXPERIMENTAL SECTION

Chemicals and materials

All chemicals were of analytical grade, purchased from Aladdin Chemicals Co. Ltd. (Shanghai, China), and used without further purification.

Catalysts preparation

TiO_2 nanotubes were synthesized by a hydrothermal approach, which has been described in detail elsewhere.[13] Briefly, 5 g of TiO_2 (anatase) powder was dispersed in 70 mL of 10 M NaOH under stirring. The mixture was then transferred into a 150 mL Teflon-lined autoclave. The autoclave was then sealed and placed at a preheated oven at 140 °C for 20 h. The precipitated powder was filtered and washed with 0.1 M HNO_3 and deionized water for several times until the filtrate solution became neutral. Then it was air-dried at 105 °C overnight. The resulting product was denoted as A-NTs. The rutile nanotubes (R-NTs) and P25 nanotubes (P-NTs) were prepared by the same procedure.

The ceria sample was prepared by a conventional precipitation method reported by our group.[14] Briefly, 5.0 g of $Ce(NO_3)_3 \cdot 6H_2O$ was dissolved in 100 mL of Millipore-purified water (18 mΩ·cm), and the solution was adjusted to pH = 10.0 by the addition of $NH_3 \cdot H_2O$ under magnetic stirring at room temperature. The resulting gel mixture was washed with pure water, dried in an oven at 120 °C overnight, and calcined at 400 °C in air for 6 h.

For ceria/A-NTs, CuO_x/A-NTs and CuO_x/ceria/A-NTs nanocomposites, a wet-chemical deposition precipitation (DP) method was employed. The preparation procedure was as follows: 0.87 g of $Ce(NO_3)_3 \cdot 6H_2O$ was dissolved in 100 mL of Millipore-purified water, and mixed with 1.6 g of the as-prepared anatase nanotubes. Sufficient $NH_3 \cdot H_2O$ (wt %: 25%−28%) was then added under vigorous stirring to adjust the pH to 10. After that, this mixture was stirred again for 5 h and then aged for 4 h without stirring at room temperature. The resulting product was filtered, dried at 105 °C overnight and calcined at 400 °C for 2 h to generate ceria/A-NTs. Other TiO_2 supported catalysts, such as CuO_x/A-NTs, CuO_x/ceria/A-NTs, ceria/R-NTs and ceria/P-NTs were prepared by the same wet-chemical DP method. Note that, for all of the catalysts, the molar ratios of Ce/Ti, Cu/Ce and Cu/Ti were 1:10, 1:4 and 1:40, respectively.

Catalyst characterizations

Powder X-ray diffraction patterns were conducted on a PANalytical X-Pert PRO diffractometer, using Cu-Kα radiation at 40 kV and 20 mA. Continuous scans were collected in the 2θ range of 10-80°.

Scanning transmission electron microscopy (STEM) was performed using a FEI Titan 80-200 (ChemiSTEM) electron microscope operated at 200 kV, equipped with a spherical-aberration (Cs) probe corrector (CEOS GmbH), and a high-angle annular dark field (HAADF) detector. A probe semi-angle of 25 mrad and an inner collection semi-angle of the detector of 88 mrad were used. Compositional maps were obtained with energy-dispersive X-ray spectroscopy (EDX) using four large-solid-angle symmetrical Si drift detectors. For EDX analysis, Cu K, Ti K, and Ce L peaks were used. High resolution transmission electron microscopy (HRTEM) investigations were performed using an FEI-Titan 80-300 electron microscope equipped with a Cs corrector for the objective lens. The microscope was operated at a voltage of 300 kV using the negative-Cs imaging technique (NCSI, with Cs set at around ~13 μm and defocus around +6 nm).

The Brunauer-Emmet-Teller (BET) surface area, total pore volume, and average pore sizes of sample were measured by N_2 adsorption and desorption on a Quadrasorb SI instrument (Quantachrome, USA) at liquid nitrogen temperature (77.3 K). Before measurement, the sample was degassed under vacuum condition at 300 °C for 5 h. The BET specific surface area was calculated from the adsorption data in the relative pressure range between 0.05 and 0.30.

Raman spectra were recorded on a confocal microscopic Raman spectrometer (Bruker Optics Senterra) using a laser with the wavelength of 532 nm.

UV-Vis diffuse reflectance spectra were recorded on JASCO V-550 UV-Vis spectrophotometer.

Photocatalytic activity tests

Photocatalytic aerobic oxidation reaction was carried out in a homemade LED photoreactor. Typically, 0.05 mmol of 1,2-diphenylethanol (substrate **1**) and 10 mg of photocatalyst were added to 1 mL of solvent in a 4 mL quartz tube. The system was replaced with O_2 for 1 min before it was sealed with a ground glass stopper and Parafilm. The quartz tube was then irradiated with 455 nm LED light. The conversion of 1,2-diphenylethanol and yield of benzaldehyde (**1a**) were determined by gas chromatography (GC) with *n*-dodecane as the internal standard. *CAUTIOUS! Specific protection by wearing eye goggle of shielding 455 nm light is mandatory to avoid injuring eyes.*

Computational method of PEDOS

All the first-principles electronic structure calculations were carried out using the Vienna ab initio simulation package (VASP),[15] one density functional theory implementation. The exchange correlation potential was described by the Perdew-Burke-Ernzerhof (PBE)[16] formulation of the generalized gradient approximation (GGA). The ion-electron interactions were represented by the projector augmented-wave (PAW)[17] method, while the valence electrons ($2s^2 2p^4$ of O, $3s^2 3p^6 3d^2 4s^2$ of Ti, and $3d^{10}4s$ of Cu) were expanded by a plane wave basis set with an energy cutoff of 400 eV. The k-point sampling was performed using the Monkhorst Pack scheme.[18] The electronic self-consistent minimization was converged to 10^{-5} eV and the geometry optimization was converged to 10^{-4} eV. The self-interaction error (SIE) was mitigated using the DFT+U method by Dudarev and his colleagues.[19] A

typical U value of 4.5 eV was used for Ti.

The lattice constants of anatase TiO_2 were optimized to be a=3.855 Å and c=9.661 Å, in good agreement with the experimental one, a=3.782 Å and c=9.502 Å.[20] We used it to build a *p*(2×4) TiO_2(101) slab with 12 atomic layers and a vacuum of 15 Å. Atoms in the bottom 6 atomic layers were fixed to their bulk positions while the rest were allowed to fully relax. A 4×3×1 k-point mesh was used.

Computational method of BDE

The Vienna Ab Initio Package (VASP)[21] was employed to perform spin-polarized DFT calculations within the generalized gradient approximation (GGA) using the PBE[22] functional formulation. The ionic cores were described by the projected augmented wave (PAW) pseudopotentials.[23] 1s of H, $2s^2 2p^2$ of C, and $2s^2 2p^4$ of O electrons were explicitly taken into account using a plane wave basis set with an energy cutoff of 400 eV. Partial occupancies of the Kohn−Sham orbitals were allowed using the Gaussian smearing method and a width of 0.05 eV. All the molecules and radicals after bond cleavage are put separately and relaxed fully in a cubic box with a side length of 20 Å. Brillouin zone integration was performed using a 2×2×2 Monkhorst-Pack grid. The electronic energy was considered self-consistent when the energy change was 10^{-7} eV. A geometry optimization was considered convergent when the energy change was 10^{-6} eV.

RESULTS AND DISCUSSION

Photocatalytic oxidation of lignin β-1 model

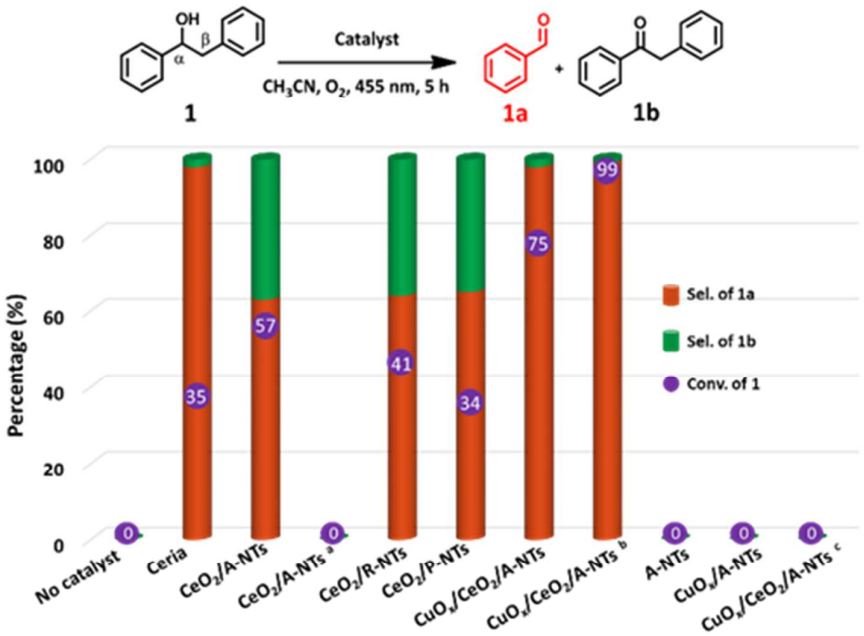

Figure 1. The photocatalytic activity of different photocatalysts for oxidation of substrate **1**. Reaction conditions: substrate **1** (0.05 mmol), catalyst (10 mg), CH_3CN (1.0 mL), O_2 (1 atm), 9.6 W LED (centered at 455 nm), room temperature, 5 h. [a] With **1b** as substrate. [b] The reaction time was 10 h. [c] The reaction was conducted in the dark. The conversion and the yields were determined by GC with *n*-dodecane as the internal standard.

We firstly explored the oxidation of 1,2-diphenylethanol under 455 nm visible light irradiation (Figure 1). The reaction did not proceed in the absence of catalyst. Pristine ceria exhibited moderate activity towards C–C bond cleavage of β-1 lignin model under visible light and gave 35% conversion of substrate **1** with 98% selectivity of C–C bond cleavage. Photocatalytic activity of ceria depends on the concentration of surface defect sites (Ce^{3+} ions and O vacancies).[24] Tuning the surface defects could tailor the photo-reactivity of ceria catalysts.[25] Aiming at achieving defected ceria, we dispersed ceria on anatase nanotubes (A-NTs) by

deposition-precipitation (DP) method with a Ce:Ti molar ratio of 1:10. The as-prepared ceria contained abundant Ce^{3+} and oxygen vacancy at the exposed interface of ceria and anatase.[13b] Expectedly, the conversion of **1** over ceria/A-NTs reached 57%. Benzaldehyde was the major product. But such a catalyst showed 37% selectivity of oxy-dehydrogenation to diphenylethanone (**1b**), indicating the ceria/A-NTs catalyst has oxy-dehydrogenation ability. Employing diphenylethanone (**1b**) as substrate gave no benzaldehyde, inferring the oxy-dehydrogenation reaction to ketone is parallel to the C–C cleavage reaction to benzaldehyde. Replacing anatase nanotubes support by rutile and P25 nanotubes slightly decreased conversion but could not increase selectivity.

In order to increase benzaldehyde selectivity, the parallel oxy-dehydrogenation reaction should be suppressed. Previous studies have shown the modification with copper oxides could alter the photocatalytic activity of TiO_2.[26] On the other hand, the copper-based catalysts are favorable for thermal oxidative cleavage of C–C bond reported by other groups and ours.[1d, 9b, 27] So we prepared a catalyst by mixing copper and cerium salt precursors and precipitating them on A-NTs by the DP method, named as CuO_x/ceria/A-NTs (2 wt% CuO loading relative to ceria/A-NTs) for this reaction. The conversion of substrate **1** increased to 75% and surprisingly with 98% selectivity of benzaldehyde. Extension of the reaction time to 10 h realized complete conversion of substrate **1** with > 99% selectivity of benzaldehyde. The oxy-dehydrogenation reaction was almost completely suppressed. Control reactions using A-NTs and CuO_x/A-NTs as catalysts under the same conditions gave no product,[28] indicating

ceria plays a key role in this photocatalytic system. Moreover, it is a photocatalytic reaction and didn't occur in the dark.

We then investigated the photo-oxidation of a more complex β-1 model 1-(3,4-dimethoxyphenyl)-2-(4-methoxyphenyl)-propane-1,3-diol (substrate **2**) with *γ*-hydroxyl and methoxyl substituents (Scheme 2). The cleavage of C–C bond offered 96% yield of veratraldehyde and >99% yield of anisic aldehyde even in the presence of *γ*–hydroxyl and methoxyl groups. The Cu/substrate ratio and temperature of reaction are lower and the yields of aromatic aldehydes are higher than using homogeneous copper catalyst.[3]

Scheme 2. Photocatalytic C–C bond cleavage of nonphenolic lignin model substrate 2 to aromatic aldehydes over CuO_x/ceria/A-NTs

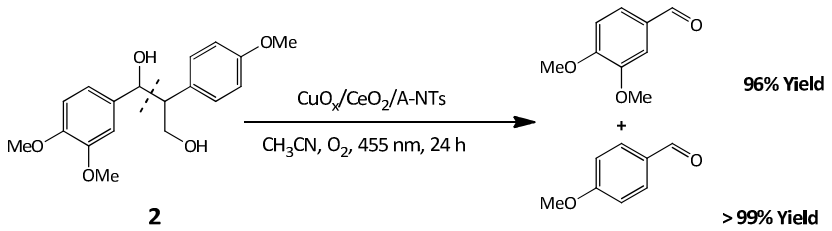

Reaction conditions: substrate **2** (0.05 mmol), CuO_x/ceria/A-NTs (10 mg), CH_3CN (1.0 mL), O_2 (1 atm), 9.6 W LED (centered at 455 nm), room temperature, 24 h. The yields of aldehydes were determined by GC with *n*-dodecane as the internal standard.

XRD and TEM characterization of the photocatalysts

Such unexpected results motivated us to investigate the structure of the catalysts. XRD diffraction patterns of the as-prepared ceria and A-NTs are dominated by the

expected lines for *fcc* fluorite CeO_2 (JCPDS: 34-0394) and anatase (JCPDS: 21-1272), respectively (Figure 2). The characteristic peaks of crystalline ceria are not observed except for a weak and broad peak at 28.6° for ceria/A-NTs and CuO_x/ceria/A-NTs. It is well accepted that if the size of crystalline particles is smaller than 4 nm, their diffraction peaks will be significantly broadened or even absent.[29] Therefore, the disappearance of ceria diffraction peaks is due to the high dispersion of ceria. After CuO_x was decorated onto ceria/A-NTs or A-NTs (2 wt% respective to ceria/A-NTs), no extra diffraction lines attributed to CuO_x were observed, indicating the high dispersion of CuO_x.

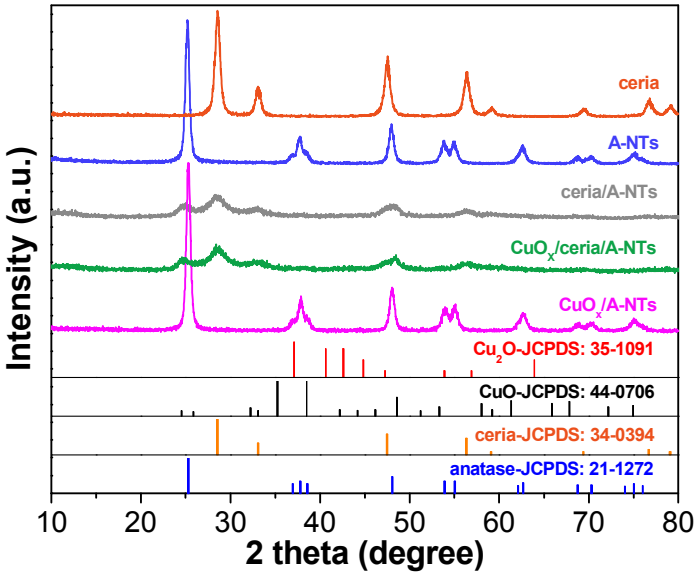

Figure 2. XRD patterns of ceria, A-NTs, ceria/A-NTs, CuO_x/ceria/A-NTs, and CuO_x/A-NTs photocatalysts, respectively.

To investigate the microstructure of the photocatalysts, HRTEM, HAADF-STEM, EDX-mapping, and fast Fourier transform (FFT) characterizations were then carried

out (Figure 3 and Figure S1). The as-prepared anatase sample has a nanotube structure with outer and inner diameters of about 10 nm and 6.5 nm, respectively (Figure S1a). The CuO_x/ceria/A-NTs consists of uniform and well-dispersed nanoparticles on the ridged surface of the anatase nanotubes. A comparison between the high-resolution STEM image (Figure 3 d) and the EDX maps confirms that the bright dots are ceria nanoparticles. The size of the ceria ranged from 2 to 8 nm with an average diameter of 4.3 nm (Figure S1 and Figure 3). The FFT image in Figure 3b displays the interplanar *d*-spacings for CeO_2 (d_{111} = 0.31 nm), TiO_2 (d_{101} = 0.35 nm), Cu_2O (d_{200} = 0.21 nm), and CuO (d_{200} = 0.23 nm and d_{110} = 0.28 nm) (Figure 3c), respectively. The STEM images and EDX mappings (Figure 3 and Figure S1d) confirm that Ce and Cu are highly dispersed on the CuO_x/ceria/A-NTs substrate. Furthermore, the EDX maps (Figure 3e-i) show that the CuO_x clusters are very finely dispersed and associated to both ceria nanoparticles and the naked anatase nanotubes. The BET surface areas and pore volume measurements by nitrogen adsorption and desorption are also conducted (Table S1). Both BET surface areas and pore volume only have a slight decline for ceria/A-NTs and CuO_x/ceria/A-NTs compared with A-NTs, indicating that most of ceria and CuO_x are present on the exterior surface of the nanotubes.

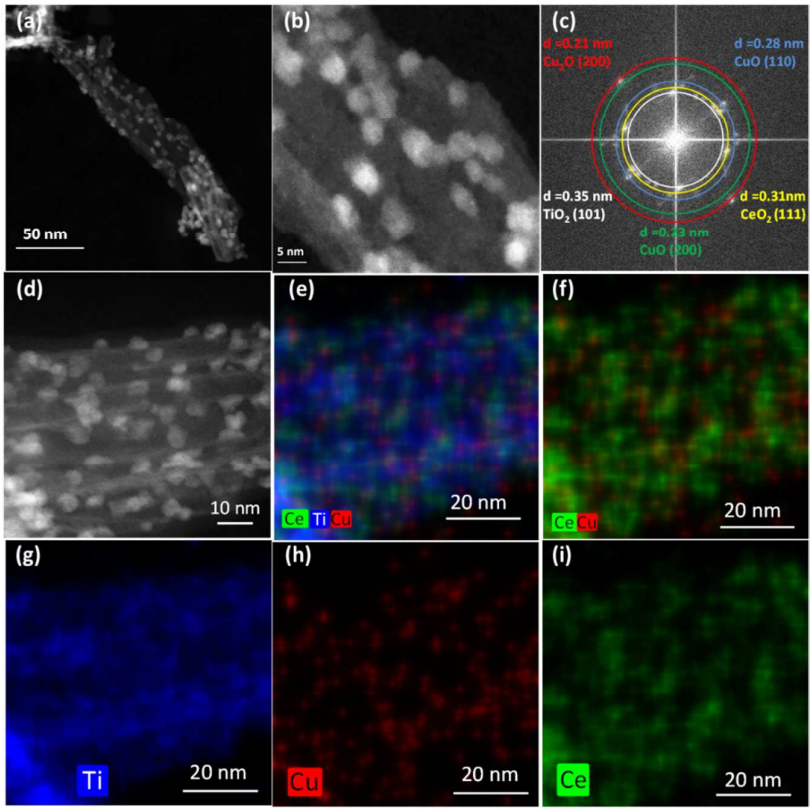

Figure 3. Low- (a) and high-resolution (b) HAADF-STEM images (c) Fast Fourier transform of image (b), (d) High-resolution HAADF-STEM image and corresponding (e-i) EDX maps of CuO_x/ceria/A-NTs.

Investigation of the reaction mechanism

Next, we turned our attention to elucidate the reaction mechanism. Effects of reaction atmosphere and trapping agents were explored to discover the key active species that oriented the reaction path (Figure 4). When the reaction was conducted in air, the yield of benzaldehyde slightly declined to 60% (Figure 4b). Moreover, the yield decreased to 9% under Ar (Figure 4c), indicating oxygen is necessary. According to previous studies, molecular oxygen could be activated to a superoxide anion radical after acquiring an excited electron from the conduction band of a

photocatalyst.[30] Adding one equivalent amount of superoxide anion radical scavenger *p*-benzoquinone (BQ)[30a] decreased the benzaldehyde yield to < 1% (Figure 4d), inferring this is a possible radical reaction.[30] Adding ammonium oxalate (AO)[30a] to capture photogenerated holes could reduce benzaldehyde yield to 1% (Figure 4e). Adding $K_2S_2O_8$[30a] to capture photogenerated electrons also led to the low yield of benzaldehyde (6%) (Figure 4f). The above results suggest that photoexcited electrons, holes and superoxide anion radical are essential species for the reaction.

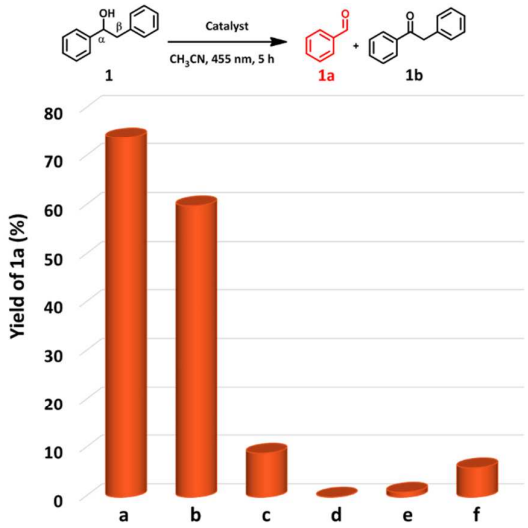

Figure 4. Influence of the reaction atmosphere and scavenger. Reaction conditions: substrate **1** (0.05 mmol), CuO_x/ceria/A-NTs (10 mg), CH_3CN (1.0 mL), reaction pressure (1 atm), additive (0.05 mmol), 9.6 W LED (centered at 455 nm), room temperature, 5 h. The yield of **1a** was determined by GC with *n*-dodecane as the internal standard. (a and d-f) Reaction under O_2. (b) Reaction under Air. (c) Reaction under Ar. (d) Reaction with *p*-benzoquinone as scavenger for superoxide radical. (e) Reaction with $(NH_4)_2C_2O_4$ as the scavenger for photogenerated holes. (f) Reaction with $K_2S_2O_8$ as the scavenger for photogenerated electrons.

Diphenylethanone (**1b**) could be oxidized to ester via C–C bond cleavage using $Cu(OAc)_2/BF_3{\cdot}OEt_2$ catalyst.[5] In this study, diphenylethanone could not be converted into benzaldehyde using the CuO_x/ceria/A-NTs catalyst (Scheme 3, Eq. 1). The results show the oxy-dehydrogenation of **1** to **1b** competes with the C–C cleavage reaction. Furthermore, we investigated the H/D KIE of the reaction (Scheme 3). When **1-D** or **1'-D** was used as substrate, the secondary kinetic isotope effect with k_H/k_D values of 1.44 and 1.23, respectively, was observed, indicating that the cleavage of O–H bond or C_α–H is not a rate-determining step (Scheme 3, Eq. 2-3). Notably, when using **1'-D** as substrate, nearly half of benzaldehyde was deuterated (Scheme 3, Eq. 3). Further experiments showed benzaldehyde could not undergo H/D exchange with 0.5 equivalent deuterated water under reaction conditions (Scheme 3, Eq. 4). These results demonstrate that C_α–H bond connecting with the hydroxyl group was retained during the C–C bond cleavage. Additionally, a first-order KIE with a value of 6.53 was observed for **1''-D** (Scheme 3, Eq. 5), implying the H-abstraction from β-C is involved in the C–C bond cleavage of substrate **1**. Oxidation of **1** to **1a** and **1b** is distinguished based on an initial hydrogen abstraction reaction at one of two positions (α-C and β-C). A benzylic radical is generated at α-C or β-C, which is resonance-stabilized by aromatic ring.

Scheme 3. Control experiment and kinetic isotope effects (KIE)

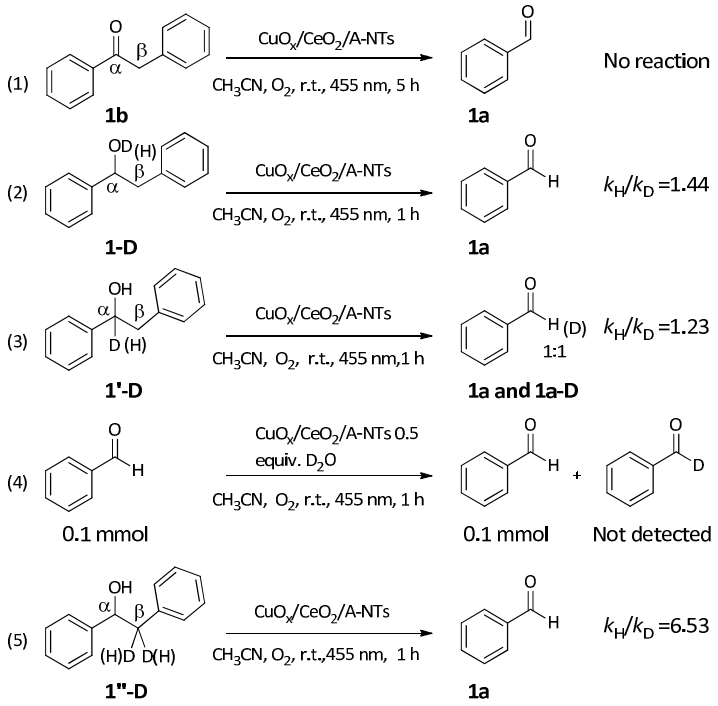

Based on the above results, we propose a tentative reaction mechanism involving hydrogen abstraction at α or β position as depicted in Scheme 4. Photogenerated electron is transferred to O_2, producing a superoxide anion radical. The hole abstracts a hydrogen from β-C to generate C_β-centered radical. The superoxide anion radical then adds to C_β-centered radical forming an unstable peroxide intermediate. The latter will undergo C_α–C_β cleavage with the elimination of H_2O to form benzaldehyde through the six-membered ring transition state (white and upper cycle). Alternatively, a radical generated at α-C will produce the diphenylethanone **1b** (dark and lower cycle).

Scheme 4. Possible mechanism.

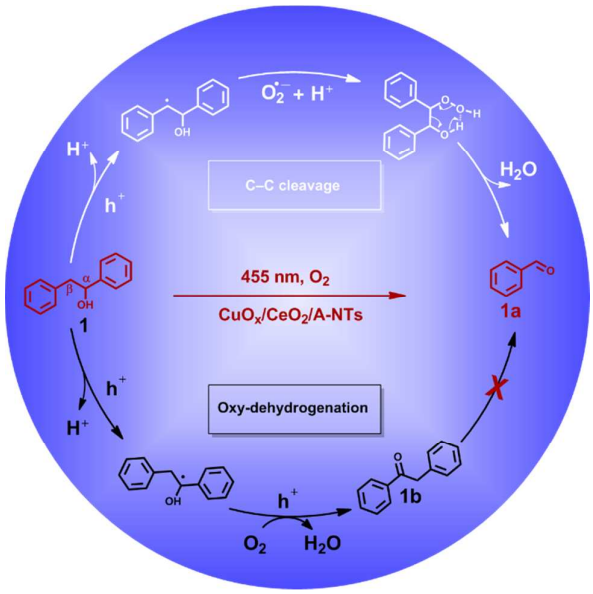

The role of the CuO_x clusters on the reaction

Furthermore, we studied the role of the CuO_x clusters on the reaction. Previous theoretical calculations and experimental studies have suggested that the photocatalytic performance of ceria is associated with the surface oxygen vacancies and Ce^{3+} ions.[25b, 31] Copper oxides could increase surface oxygen vacancies and Ce^{3+} ions of ceria in the case of CuO_x/CeO_2.[32] Ce^{3+} ions are generated by reducing Ce^{4+} ions when the oxygen vacancy is created.[33] The concentration of surface oxygen vacancies can be semi-quantified by Raman spectroscopy.[14, 34] We adopted a method[35] by using the Raman peak centered at 462 cm^{-1} to estimate the oxygen vacancy concentration of ceria. The results were presented in Figure 5b. The oxygen vacancy concentration of pristine ceria is 3.58×10^{21} cm^{-3}. A higher value of 5.88×10^{21} cm^{-3}

is obtained when ceria is highly dispersed in nanosized domains on anatase nanotubes. More oxygen vacancy (6.04×10^{21} cm^{-3}) is generated after mixing copper oxide with ceria.

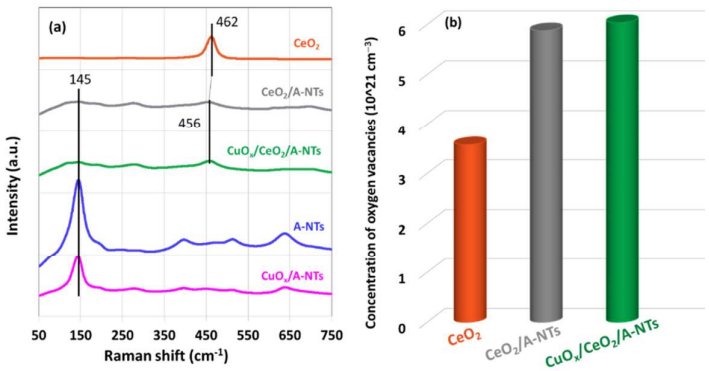

Figure 5. Raman spectra (a) and the oxygen vacancy concentration (b) of the photocatalysts.

Next we measured the UV-vis spectra to study the optical properties of photocatalysts (Figure 6). A-NTs have no significant absorption of visible light owing to its large energy gap. However, the addition of ceria extends the absorption of the resulting catalysts to visible light, which was also observed by other studies.[31a, 31b] This visible absorption enhancement could be attributed to the existence of oxygen vacancies and Ce^{3+} ions. The positive correlation between absorption at 455 nm and the concentration of oxygen vacancies and Ce^{3+} ions for ceria-based photocatalysts further confirms this point (Figure 6a). The calculated band gaps of the as-prepared samples using the transformed Kubelka-Munk plot are shown in Figure 6b.[36] The optical band energies of ceria/A-NTs and CuO_x/ceria/A-NTs are calculated to be 2.72 eV and 2.62 eV, respectively, which are lower than that of pristine ceria (2.86 eV). The presence of Ce^{3+} leads to the narrowing of the band gap of ceria. The CuO_x

clusters present on the ceria domains increase the concentration of surface defects (Ce^{3+} ions and oxygen vacancies), which we term its Yang character. For CuO_x/A-NTs, the band gap is 2.58 eV, lower than that of A-NTs. This result suggests copper oxide electronically modifies anatase nanotubes, which agrees with XRD, STEM and Raman spectroscopy results.

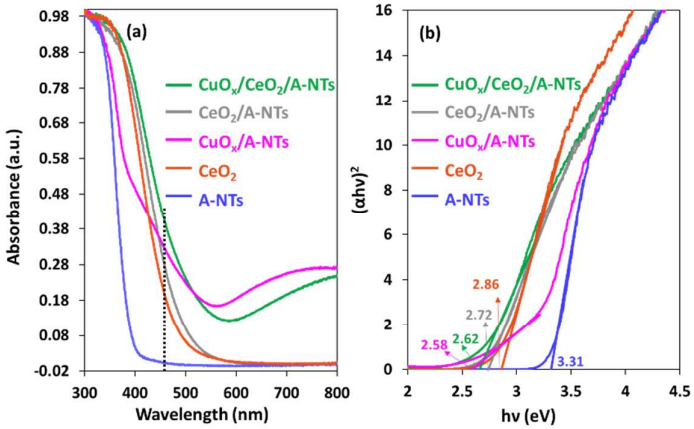

Figure 6. (a) UV–vis diffuse reflectance spectra and (b) the optical adsorption edges of the ceria, A-NTs, ceria/A-NTs, CuO_x/A-NTs and CuO_x/ceria/A-NTs photocatalysts, respectively.

CuO_x/A-NTs showed no photocatalytic activity towards the C–C bond cleavage. We then conducted a photocatalytic reaction under 365 nm UV light (Figure 7), under which electron-hole pairs of A-NTs can be excited. Consequently, the 50% yield of **1b** is obtained, together with 30% yield of **1a**, indicating both C–C bond cleavage and oxy-dehydrogenation reactions occur on anatase. Because ceria has no photocatalytic ability of oxy-dehydrogenation, it is very likely that the oxy-dehydrogenation reaction mainly occurs on A-NTs. The decoration of copper oxides on A-NTs can remarkably suppress the side reaction, decreasing yield of **1b** to 4%, which we term Yin character

of CuO_x clusters. We further compare the activities of the ceria/A-NTs and CuO_x/ceria/A-NTs under 365 nm UV light. The yield of **1a** increases from 32% to 43% and the yield of **1b** declines from 20% to 5%, which further confirms the Yin (inhibit the side oxy-dehydrogenation reaction) and Yang (enhance the C–C cleavage activity) dual characters of the CuO_x. Tada's group has observed that with the increasing loading amount of NiO_x or CuO_x nanoclusters on TiO_2, the activity of photodegradation of organics decreased.[26a, 37] In this work, we find the photocatalytic oxy-dehydrogenation reaction on anatase fades away with increasing the amount of CuO_x to 2 wt% (Table S2).

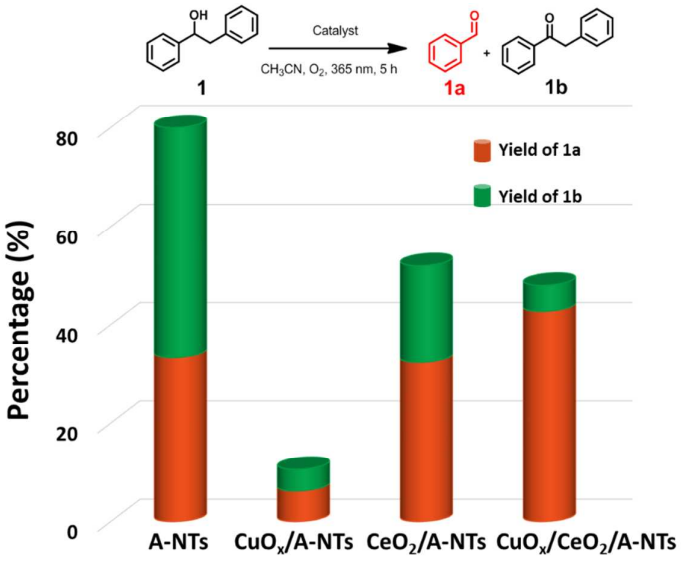

Figure 7. Photocatalytic reaction under UV light. Reaction conditions: substrate (0.05 mmol), catalyst (10 mg), CH_3CN (1.0 mL), O_2 (1 atm), 6 W LED (centered at 365 nm), room temperature, 5 h. The yields were determined by GC with *n*-dodecane as the internal standard.

To further understand the Yin character of CuO_x nanoclusters, we calculated the

partial electronic density of states (PEDOS) of CuO_x/anatase using Cu_3O_3/anatase (101) as model by DFT, in which Cu3d, O2p, and Ti3d PEDOS are displayed (Figure 8). New states are present above the valence band edge of the anatase (101) surface (Figure 8d), which arise from the presence of CuO_x-derived occupied states that lie at higher energy than the VB edge of the anatase. The upward shift in the VB edge results in a narrowing of the band gap compared to unmodified TiO_2, which is consistent with the result of UV-vis. Moreover, the rise in the VB edge will lead to the decrease of the activity of holes. As a result, the oxy-dehydrogenation reaction occurring on anatase is suppressed (Figure 7). This result is in consistency with the case of NiO_x or CuO_x nanoclusters supported on TiO_2 reported by Nolan and Tada's group.[26a, 37-38]

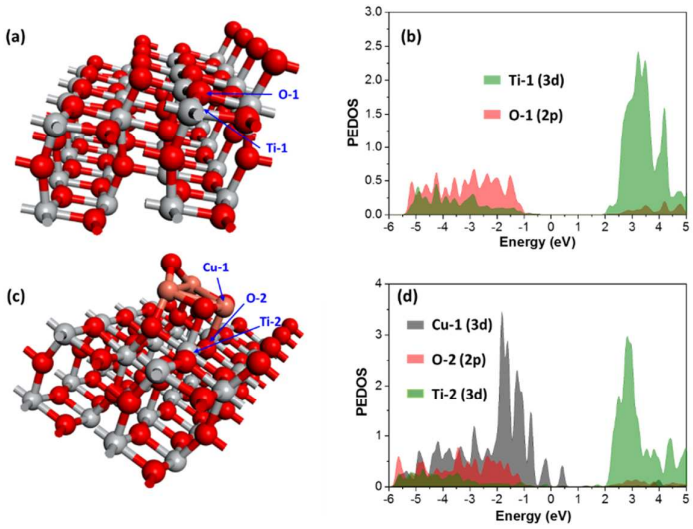

Figure 8. Atomic structure and calculated partial electronic density of states (PEDOS) for anatase (101), and Cu_3O_3/anatase (101), respectively.

CONCLUSIONS

In conclusion, we report a strategy of controlling CuO_x clusters' distribution on ceria/anatase nanotube and the catalytic consequence in the model lignin C-C bond cleavage reaction. CuO_x/ceria/A-NTs photocatalyst shows high activity in the C–C bond cleavage to benzaldehydes under visible light irradiation. Highly dispersed CuO_x clusters on ceria domains enhance the Ce^{3+} concentration in ceria, and thus increase the catalytic activity (Yang character); the decoration of CuO_x on the exposed anatase surface suppresses the unwanted oxy-dehydrogenation reaction by shifting the valence band edge of TiO_2 to higher energy (Yin character). Thus, the high photocatalytic performance is achieved under visible light. A hydrogen-abstraction by photogenerated hole is involved in the reaction mechanism. We believe this work is instructive for designing active photocatalysts for oxidation of C–C bond and valorization of lignin, as well as can be used in broad organic reactions.

AUTHOR INFORMATION

***Corresponding author:**

Feng Wang

Tel: +86-411-84379762; Fax: +86-411-84379798;

E-mail: wangfeng@dicp.ac.cn

Notes

The authors declare no competing financial interest.

ACKNOWLEDGEMENTS

This work was supported by the National Natural Science Foundation of China

(21422308, 21690082, 21690084), and the Strategic Priority Research Program of Chinese Academy of Sciences (XDB17020300). Computing resources from the National Supercomputing Center in Shenzhen (China) and National Supercomputing Center in Tianjin (China) were gratefully acknowledged.

SUPPORTING INFORMATION AVAILABLE

This material is available free of charge via the Internet at http://pubs.acs.org.

Catalyst characterization, including TEM images and physical absorption, the effect of the copper amount on photocatalytic C–C bond cleavage and the procedure for synthesis of model compounds (NMR characterization was also involved).

REFERENCES

(1) (a) Zhang, L.; Bi, X.; Guan, X.; Li, X.; Liu, Q.; Barry, B. D.; Liao, P. *Angew. Chem., Int. Ed.* **2013**, *125*, 11513-11517; (b) Souillart, L.; Cramer, N. *Chem. Rev.* **2015**, *115*, 9410-9464; (c) Huang, X.; Li, X.; Zou, M.; Song, S.; Tang, C.; Yuan, Y.; Jiao, N. *J. Am. Chem. Soc.* **2014**, *136*, 14858-14865; (d) Wang, M.; Lu, J.; Zhang, X.; Li, L.; Li, H.; Luo, N.; Wang, F. *ACS Catal.* **2016**, *6*, 6086-6090.

(2) Bharathi, K.; Ravindra, P. *Electron. J. Environ., Agric. Food Chem.* **2006**, *5*, 1253-1264.

(3) Sedai, B.; Díaz-Urrutia, C.; Baker, R. T.; Wu, R.; Silks, L. A. P.; Hanson, S. K. *ACS Catal.* **2013**, *3*, 3111-3122.

(4) Luo, F. X.; Zhou, T. G.; Li, X.; Luo, Y. L.; Shi, Z. J. *Org. Chem. Front.* **2015**, *2*, 1066-1070.

(5) Wang, M.; Li, L. H.; Lu, J. M.; Li, H. J.; Zhang, X. C.; Liu, H. F.; Luo, N. C.; Wang, F. *Green Chem.* **2016**, *19*, 702-706.

(6) (a) Tomita, O.; Otsubo, T.; Higashi, M.; Ohtani, B.; Abe, R. *ACS Catal.* **2016**, *6*, 1134-1144; (b) Higashi, M.; Domen, K.; Abe, R. *J. Am. Chem. Soc.* **2013**, *135*, 10238-10241; (c) Abe, R.; Shinmei, K.; Koumura, N.; Hara, K.; Ohtani, B. *J. Am. Chem. Soc.* **2013**, *135*, 16872-16884; (d) Barreca, D.; Fornasiero, P.; Gasparotto, A.; Gombac, V.; Maccato, C.; Montini, T.; Tondello, E. *ChemSusChem* **2009**, *2*, 230-233.

(7) (a) Gombac, V.; Sordelli, L.; Montini, T.; Delgado, J. J.; Adamski, A.; Adami, G.; Cargnello, M.; Bernal, S.; Fornasiero, P. *J. Phys. Chem. A* **2010**, *114*, 3916-3925; (b) Okunaka, S.; Tokudome, H.; Hitomi, Y.; Abe, R. *J. Mater. Chem. A* **2015**, *3*, 1688-1695; (c) Yamauchi, M.; Abe, R.; Tsukuda, T.; Kato, K.; Takata, M. *J. Am. Chem. Soc.* **2011**, *133*, 1150-1152; (d) Abe, R.; Takami, H.; Murakami, N.; Ohtani, B. *J. Am. Chem. Soc.* **2008**, *130*, 7780–7781; (e) Yurdakal, S.; Palmisano, G.; Loddo, V.; Augugliaro, V.; Palmisano, L. *J. Am. Chem. Soc.* **2008**,

130, 1568-1569.
(8) (a) Nguyen, J. D.; Matsuura, B. S.; Stephenson, C. R. *J. Am. Chem. Soc.* **2014**, *136*, 1218-1221; (b) Karkas, M. D.; Bosque, I.; Matsuura, B. S.; Stephenson, C. R. *Org. Lett.* **2016**, *18*, 5166-5169; (c) Gazi, S.; Hung Ng, W. K.; Ganguly, R.; Putra Moeljadi, A. M.; Hirao, H.; Soo, H. S. *Chem. Sci.* **2015**, *6*, 7130-7142.
(9) (a) Reddy, G. V. B.; Sridhar, M.; Gold, M. H. *Eur. J. Biochem.* **2003**, *270*, 284-292; (b) Wang, M.; Lu, J.; Ma, J.; Zhang, Z.; Wang, F. *Angew. Chem., Int. Ed.* **2015**, *54*, 14061-14065; (c) Cho, S. H.; Kim, J. Y.; Kwak, J.; Chang, S. *Chem. Soc. Rev.* **2011**, *40*, 5068-83.
(10) (a) Zhang, C.; Lu, J.; Zhang, X.; MacArthur, K.; Heggen, M.; Li, H.; Wang, F. *Green Chem.* **2016**, *18*, 6545-6555; (b) Kim, S.; Chmely, S. C.; Nimlos, M. R.; Bomble, Y. J.; Foust, T. D.; Paton, R. S.; Beckham, G. T. *J. Phys. Chem. Lett.* **2011**, *2*, 2846-2852.
(11) (a) Lim, S. H.; Lee, W. S.; Kim, Y.-I.; Sohn, Y.; Cho, D. W.; Kim, C.; Kim, E.; Latham, J. A.; Dunaway-Mariano, D.; Mariano, P. S. *Tetrahedron* **2015**, *71*, 4236-4247; (b) Cho, D. W.; Parthasarathi, R.; Pimentel, A. S.; Maestas, G. D.; Park, H. J.; Yoon, U. C.; Dunaway-Mariano, D.; Gnanakaran, S.; Langan, P.; Mariano, P. S. *J. Org. Chem.* **2010**, *75*, 6549-62.
(12) In Chinese philosophy, Yin means the negative principle (characterized by dark) and Yang means the positive principle (characterized by light) of the two opposing cosmic forces. Yin and yang describe how seemingly opposite or contrary forces may actually be complementary, interconnected, and interdependent in the natural world, and how they may give rise to each other as they interrelate to one another. In this work, the decorated of CuOx clusters could suppress the oxy-dehydrogenation reaction, which we termed it Yin character and promoted the C–C bond cleavage, which we termed it Yang character.
(13) (a) Tsai, C.; Teng, H. *Chem. Mater.* **2004**, *16*, 4352-4358; (b) Zhao, H.; Dong, Y.; Jiang, P.; Wang, G.; Zhang, J. *ACS Appl. Mater. Interfaces* **2015**, *7*, 6451-6461.
(14) Wang, Y.; Wang, F.; Song, Q.; Xin, Q.; Xu, S.; Xu, J. *J. Am. Chem. Soc.* **2013**, *135*, 1506-1515.
(15) Kresse, G.; Furthmuller, J. *Comput. Mater. Sci.* **1996**, *6*, 15-50.
(16) Perdew, J. P.; Burke, K.; Ernzerhof, M. *Phys. Rev. Lett.* **1996**, *77*, 3865.
(17) Kresse, G.; Joubert, D. *Phys. Rev. B* **1999**, *59*, 1758-1775.
(18) Monkhorst, H. J.; Pack, J. D. *Phys. Rev. B* **1976**, *13*, 5188-5192.
(19) Dudarev, S. L.; Botton, G. A.; Savrasov, S. Y.; Humphreys, C. J.; Sutton, A. P. *Phys. Rev. B* **1998**, *57*, 1505-1509.
(20) Burdett, J. K.; Hughbanks, T.; Miller, G. J.; Richardson, J. W.; Smith, J. V. *J. Am. Chem. Soc.* **1987**, *109*, 3639-3646.
(21) (a) Kresse, G.; Furthmuller, J. *Phys. Rev. B* **1996**, *54*, 11169-11186; (b) Kresse, G.; Furthmuller, J. *Comput. Mater. Sci.* **1996**, *6*, 15-50.
(22) Perdew, J. P.; Burke, K.; Ernzerhof, M. *Phys. Rev. Lett.* **1996**, *77*, 3865-3868.
(23) (a) Kresse, G.; Joubert, D. *Phys. Rev. B* **1999**, *59*, 1758-1775; (b) Blochl, P. E. *Phys. Rev. B* **1994**, *50*, 17953-17979.
(24) (a) Jiang, D.; Wang, W.; Zhang, L.; Zheng, Y.; Wang, Z. *ACS Catal.* **2015**, *5*, 4851-4858; (b) Khan, M. M.; Ansari, S. A.; Pradhan, D.; Han, D. H.; Lee, J.; Cho, M. H. *Ind. Eng. Chem. Res.* **2014**, *53*, 9754-9763.
(25) (a) Younis, A.; Chu, D.; Kaneti, Y. V.; Li, S. *Nanoscale* **2016**, *8*, 378-387; (b) Zhao, K.; Qi, J.; Yin, H.; Wang, Z.; Zhao, S.; Ma, X.; Wan, J.; Chang, L.; Gao, Y.; Yu, R.; Tang, Z. *J. Mater.*

Chem. A **2015**, *3*, 20465-20470; (c) Andersson, D. A.; Simak, S. I.; Johansson, B.; Abrikosov, I. A.; Skorodumova, N. V. *Phys. Rev. B* **2007**, *75*, 035109; (d) Montini, T.; Melchionna, M.; Monai, M.; Fornasiero, P. *Chem. Rev.* **2016**, *116*, 5987-6041.

(26) (a) Jin, Q.; Fujishima, M.; Iwaszuk, A.; Nolan, M.; Tada, H. *J. Phys. Chem. C* **2013**, *117*, 23848-23857; (b) Assadi, M. H. N.; Hanaor, D. A. H. *Appl. Surf. Sci.* **2016**, *387*, 682-689.

(27) Tang, C.; Jiao, N. *Angew. Chem., Int. Ed.* **2014**, *53*, 6528-6532.

(28) If the reaction was conducted under 365 nm light illumination, the substrate 1a was dehydrogenated to 1b as major product over A-NTs, as shown in Figure 8.

(29) Zhao, J.; Chen, H.; Tian, X.; Zang, H.; Fu, Y.; Shen, J. *J. Catal.* **2013**, *298*, 161-169.

(30) (a) Raza, F.; Park, J. H.; Lee, H.; Kim, H.; Jeon, S.; Kim, J. *ACS Catal.* **2016**, *6*, 2754-2759; (b) Lang, X.; Ji, H.; Chen, C.; Ma, W.; Zhao, J. *Angew. Chem., Int. Ed.* **2011**, *50*, 3934-3937; (c) Su, F.; Mathew, S. C.; Mohlmann, L.; Antonietti, M.; Wang, X.; Blechert, S. *Angew. Chem., Int. Ed.* **2011**, *50*, 657-660.

(31) (a) Luo, S.; Nguyen-Phan, T.-D.; Johnston-Peck, A. C.; Barrio, L.; Sallis, S.; Arena, D. A.; Kundu, S.; Xu, W.; Piper, L. F. J.; Stach, E. A.; Polyanskiy, D. E.; Fujita, E.; Rodriguez, J. A.; Senanayake, S. D. *J. Phys. Chem. C* **2015**, *119*, 2669-2679; (b) Wang, Y.; Zhao, J.; Wang, T.; Li, Y.; Li, X.; Yin, J.; Wang, C. *J. Catal.* **2016**, *337*, 293-302; (c) Kundu, S.; Ciston, J.; Senanayake, S. D.; Arena, D. A.; Fujita, E.; Stacchiola, D.; Barrio, L.; Navarro, R. M.; Fierro, J. L. G.; Rodriguez, J. A. *J. Phys. Chem. C* **2012**, *116*, 14062-14070; (d) Catlow, C. R.; Guo, Z. X.; Miskufova, M.; Shevlin, S. A.; Smith, A. G.; Sokol, A. A.; Walsh, A.; Wilson, D. J.; Woodley, S. M. *Philos. Trans. R. Soc. A* **2010**, *368*, 3379-456.

(32) Knauth, P.; Saltsburg, H.; Engel, J.; Tuller, H. L. *J. Mater. Chem. A* **2015**, *3*, 8369-8379.

(33) (a) Lee, Y.; He, G.; Akey, A. J.; Si, R.; Flytzani-Stephanopoulos, M.; Herman, I. P. *J. Am. Chem. Soc.* **2011**, *133*, 12952-12955; (b) Esch, F.; Fabris, S.; Zhou, L.; Montini, T.; Africh, C.; Fornasiero, P.; Comelli, G.; Rosei, R. *Science* **2005**, *309*, 752-755.

(34) (a) Wu, Z.; Li, M.; Howe, J.; Meyer III, H. M.; Overbury, S. H. *Langmuir* **2010**, *26*, 16595-16606; (b) Li, M.; Tumuluri, U.; Wu, Z.; Dai, S. *ChemSusChem* **2015**, *8*, 3651-3660; (c) Wu, Z.; Li, M.; Overbury, S. H. *ChemCatChem* **2012**, *4*, 1653-1661; (d) Zhang, L.; Wu, Z.; Nelson, N. C.; Sadow, A. D.; Slowing, I. I.; Overbury, S. H. *ACS Catal.* **2015**, *5*, 6426-6435; (e) Zhang, Z.; Wang, Y.; Wang, M.; Lu, J.; Li, L.; Zhang, Z.; Li, M.; Jiang, J.; Wang, F. *Chin. J. Catal.* **2015**, *36*, 1623-1630; (f) Zhang, Z.; Wang, Y.; Wang, M.; Lu, J.; Zhang, C.; Li, L.; Jiang, J.; Wang, F. *Catal. Sci. Technol.* **2016**, *6*, 1693-1700.

(35) (a) Deori, K.; Gupta, D.; Saha, B.; Deka, S. *ACS Catal.* **2014**, *4*, 3169-3179; (b) Trogadas, P.; Parrondo, J.; Ramani, V. *ACS Appl. Mater. Interfaces* **2012**, *4*, 5098-5102.

(36) Saavedra, J.; Doan, H. A.; Pursell, C. J.; Grabow, L. C.; Chandler, B. D. *Science* **2014**, *345*, 1599-1602.

(37) Iwaszuk, A.; Nolan, M.; Jin, Q.; Fujishima, M.; Tada, H. *J. Phys. Chem. C* **2013**, *117*, 2709-2718.

(38) (a) Fronzi, M.; Iwaszuk, A.; Lucid, A.; Nolan, M. *J. Phys.: Condens. Matter* **2016**, *28*, 074006; (b) Nolan, M.; Iwaszuk, A.; Lucid, A. K.; Carey, J. J.; Fronzi, M. *Adv. Mater.* **2016**, *28*, 5425-5446.

TOC

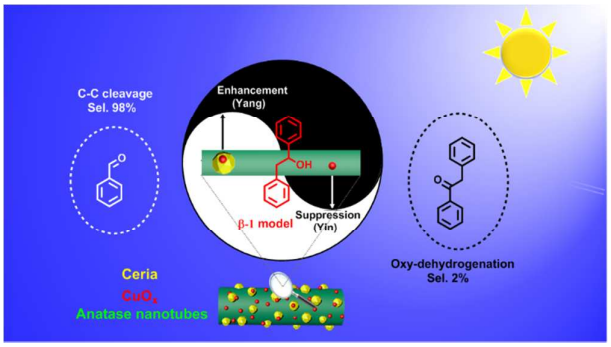
C-C cleavage
Sel. 98%
Enhancement
(Yang)
OH
β-I model
Suppression
(Yin)
Oxy-dehydrogenation
Sel. 2%
Ceria
CuO_x
Anatase nanotubes